Evolution dynamics of charge state distribution in neon interaction with x-ray pulses of variant intensities and durations

Article *in* High Energy Density Physics · March 2015

Impact Factor: 1.23 · DOI: 10.1016/j.hedp.2015.03.003

3 authors, including:

Cheng Gao

National University of Defense Technology

25 PUBLICATIONS **74** CITATIONS

SEE PROFILE

Jianmin Yuan

National University of Defense Technology

233 PUBLICATIONS **1,858** CITATIONS

SEE PROFILE

Evolution dynamics of charge state distribution in neon interaction with x-ray pulses of variant intensities and durations

Cheng Gao[a], Jiaolong Zeng[a,*], Jianmin Yuan[a,b,*]

[a] *College of Science, National University of Defense Technology, Changsha Hunan 410073, P. R. China*
[b] *IFSA Collaborative Innovation Center, Shanghai Jiao Tong University, Shanghai 200240, P. R. China*

Abstract

The level population and charge state distribution (CSD) of the neon atomic system interacting with x-ray pulses of variant intensities and durations at a central photon energy of 1110 eV are investigated by solving the time-dependent rate equations. The laser beam has a circular spot size with a Gaussian intensity pattern and the time history of the intensity is represented by Gaussian distribution in time. As an example, the CSD as a function of time is given at different distances from the spot center for an x-ray beam of intensity 1.5×10^{17} W/cm^2 and duration 75 femtosecond (fs) for a spot size of 1 μm (full width at half maximum). The final CSD after averaging over the space and time is compared with a recent experiment and good agreement is found between the theory and experiment. Then systematic investigations are carried out to study the evolution of CSD with a wide range of intensity from 1.0×10^{15} W/cm^2 to 1.0×10^{19} W/cm^2 and duration from 30 fs to 100 fs. The results show that at intensities lower than 1.0×10^{15} W/cm^2, the CSD shows a typical physical picture of weak x-ray photoionization of the neutral atomic neon. At higher intensity, i.e., larger than 5.0×10^{16} W/cm^2, the dominant ionization stages are Ne^{7+} and Ne^{8+}, while the fractions of ions in the Ne^{3+}-Ne^{6+} stages are low for all laser durations and intensities.

Keywords: charge state distribution, rate equation, x-ray laser-matter interaction

1. Introduction

X-ray free-electron lasers such as the Linac Coherent Light Source (LCLS) [1] and the Spring-8 Angstrom Compact free electron LAser (SACLA) [2] open new possibility to investigate the physics of light-matter interaction in the short-wavelength regime at ultra-high intensity of $\sim10^{19}$ W/cm^2. A series of experiments [3–11] showed that the x-ray absorption is dominated by single photon ionization of deep inner-shell electrons yet resonance absorption [10, 12] and two-photon absorption [6] play a role. These pioneering experiments investigated photoabsorption mechanisms by measuring the charge state distributions (CSD), which is of fundamental importance for any further studies such as equation of state and radiative

*Corresponding author
Email addresses: jlzeng@nudt.edu.cn (Jiaolong Zeng), jmyuan@nudt.edu.cn (Jianmin Yuan)

property. These studies give us an understanding of the atomic response and absorption mechanism in the interaction of ultra-intense x-ray laser pulses with matters.

In the above experiments, there is a strong need to determine the physical parameters of the laser pulses such as the duration and intensity. However, accurate measurement of the duration and intensity of ultra-intense x-ray laser pulses is challenging. In the experiments, the duration of electron bunch and pulse energy can usually be accurately measured. Yet x-ray pulse duration is different from that of the electron bunch and their quantitative relation is difficult to measure. As a result, the intensity of x-ray laser pulses is usually difficult to be experimentally determined. Thus, it is necessary to develop reliable models with accurate atomic data as input to aid the experimental analysis and to infer or diagnose the x-ray pulse intensity. Such a requirement can easily be seen from the most recent experimental work on the interaction of high x-ray laser fluence with a liquid water jet [11]. Schreck *et al.* [11] reported on oxygen K-edge soft x-ray emission spectroscopy from a liquid water jet at LCLS. Significant changes in the spectral characteristics are found when they change the laser intensity. The authors explained these modifications are due to the reabsorption of x-ray emission by the quantum states generated by sequential Auger cascade. To quantify the reabsorption mechanism, one needs detailed and accurate model to describe the trend of population distribution with the variation of the laser intensity. However, such a quantitative and systematic theoretical investigations are lacking.

Hence it is worthwhile to systematically study the dynamics of atoms over a wide range of laser intensity and duration. In this work, we utilize a detailed level accounting (DLA) model to describe the interaction of x-ray radiation with atoms. A time-dependent rate equation (TDRE) approach [13, 14] based on the collisional-radiative model is employed to obtain the CSD. The DLA method has been used to calculate the radiative opacity of hot dense plasmas in local thermodynamic equilibrium (LTE) [15–17]. Such a DLA formalism is also needed and more challenging for the highly transient plasmas produced by ultra-intense x-ray laser pulses. On one hand, more atomic data including the level-to-level excitation and ionization processes due to photons and electrons and Auger decay rate are required. On the other hand, the x-ray radiation excites and ionizes the deep inner-shell electrons and thus the atomic data such as Auger decay rates and photoionization cross sections for these highly excited states are difficult to be calculated accurately. Based on the DLA model, we systematically investigated the population dynamics for the interaction of x-ray laser pulses of different duration and intensity with neon. To have a more suitable description of the interaction of radiation and matters, we take the spatial distribution of the laser spot size and the energy spread of the incident x-ray laser beam into account. The energy spread of the laser beam is assumed to have a bandwidth of 0.5%.

2. Theoretical method

The TDRE approach is employed to study the dynamics of level population and CSD in the interaction of x-ray radiation with matters, where the rate coefficients are determined by the cross sections of microscopic processes due to photons and electrons [18, 19]. The

evolution of the population for level i in the matter system is determined by

$$\frac{dn_i}{dt} = \sum_{j\neq i}^{N_L} n_j R_{ji} - n_i \sum_{j\neq i}^{N_L} R_{ij}, \tag{1}$$

where n_i is the population of level i and R_{ij} and R_{ji} represent the rate coefficients which depopulate and populate for the level i, respectively, and N_L is the total number of levels included in the rate equation. In this work, the levels of all ionization stages from the neutral to the fully stripped neon ions are included. The details of included levels in this work will be given in the following. Explicitly, photo-excitation, photoionization, electron impact excitation, electron impact ionization, Auger decay and their inverse processes are taken into account.

The rate coefficients contributed by the photo-excitation and photoionization processes are closely related with the radiation intensity. As we know, the intensity is in general a function of space, time and frequency of x-ray pulses. In principle, the intensity distribution with the space, time and frequency can be determined experimentally. However, such measurements are challenging at the level where femtosecond x-ray pulses are being used. In the present work, we assume the laser intensity has a Gaussian profile on space, time and frequency

$$I(r,t,h\nu) = I_0 e^{-\ln 2(\frac{r}{\Delta})^2} e^{-\ln 2(\frac{t-t_0}{\tau})^2} \sqrt{\frac{\ln 2}{\pi\Gamma^2}} e^{-\ln 2(\frac{h\nu-h\nu_0}{\Gamma})^2}, \tag{2}$$

where I_0 is the peak intensity, t_0 is the center of temporal profile and $h\nu_0$ is the central photon energy of the x-ray pulse. Δ, τ and Γ are the half width at half maximum (HWHM) of Gaussian profile of the x-ray pulse for the distribution with respect to space, time and photon energy, respectively. Note that the dependence of intensity on photon energy (frequency) has been multiplied by a constant quantity to satisfy the normalization (to 1). The pulse energy of x-ray beams can be obtained by the integration over space, time and photon energy. The quantitative connection of pulse energy and intensity can help us better understand the physics of the interaction.

The rate coefficients used in the rate equation are determined by the cross sections of microscopic processes due to photons and electrons. The photoexcitation and photoionization rates $R_{ij}(r,t)$ from level i to level j irradiated by an x-ray pulse with intensity $I(r,t,h\nu)$ at spatial position r from the center of the laser spot and time t are obtained by [20]

$$R_{ij}(r,t) = \int \frac{I(r,t,h\nu)}{h\nu} \sigma_{ij}(h\nu) d(h\nu), \tag{3}$$

where $\sigma_{ij}(h\nu)$ is the photoexcitation or photoionization cross section at photon energy $h\nu$.

For electron impact excitation and ionization, the rate can be written

$$R^e_{ij} = n_e \int v(\varepsilon) f(\varepsilon) \sigma^e_{ij}(\varepsilon) d\varepsilon, \tag{4}$$

where $\sigma^e_{ij}(\varepsilon)$ means the cross section of electron impact excitation or ionization at electron energy ε, n_e is the electron density, and $f(\varepsilon)$ is the electron energy distribution function.

In principle, $f(\varepsilon)$ should be obtained by solving the Boltzmann equations for the electrons that is coupled to the rate equations [21, 22]. The evolution of $f(\varepsilon)$ with time is expressed as

$$\frac{df(\varepsilon)}{dt} = S(f(\varepsilon), \mathbf{N}), \tag{5}$$

where $\mathbf{N}$ is the population distributions of levels obtained by solving rate equation and S is the source function which is contributed by elastic and inelastic collisions. The elastic electron-electron contribution can be evaluated by using the Fokker-Planck equation and the inelastic contribution includes the microscopic atomic processes involving photons and electrons as mentioned above for the rate equation. The detailed descriptions for the construction of S can be found in Ref.[22].

3. Atomic model and atomic data

To consider all possible channels due to photo-excitation, photoionization and Auger decay, we include the quantum states of excitation of up to two $1s$ electrons from the respective ground configuration for all ionization stages from the neutral atom to bare ion in the rate equation. Explicitly, the fine structure levels belonging to the configurations of respective neon ions given in table 1 are used to construct the rate equation. In this table, we have used a simplified notation to designate the configurations. $(N)^M$ means possible arrangement of the M electrons in the orbital with principle quantum number N. For examples, $(1)^2(2)^6(3)^1$ in Ne^{1+} includes configurations of $1s^22s^22p^43l$, $1s^22s2p^53l$, and $1s^22p^63l$ ($l = s$, p, and d), which has a total number of 9 configurations. The designations beginning with $(1)^1$ and $(1)^0$ in table 1 means single and double K-shell core-hole states. The x-ray radiation effectively photoionizes the inner-shell electrons and then the single core-hole states relax dominantly by Auger decay. If the intensity is large enough, the K-shell electron of the single core-hole states will be further photoionized and hence double core-hole states are produced. Therefore, the single and double core-hole states must be included in the evolution dynamics. As is well known, the atomic data of the core-hole states, in particular the double core-hole states, are difficult to be accurately determined. The accuracy of our calculated atomic data is checked by close-coupling R-matrix formalism [23, 24].

The atomic data, including the spontaneous radiative decay rate, photoionization and photo-excitation cross section, electron impact excitation and ionization cross section and Auger decay rate connecting all the levels given in table 1, are obtained by a relativistic approach based on the Dirac equation [25]. Briefly, the relativistic Hamiltonian is our starting point to obtain the radial orbitals for the construction of basis states from a modified self-consistent Dirac-Fock-Slater iteration on a fictitious mean configuration with fractional occupation numbers. Configuration interaction between the levels belonging to the configurations given in table 1 is included to obtain as accurate atomic data as possible. The continuum wavefunction for the free electron is treated by the distorted wave approximation. Here we do not give any theoretical details, which can be found in Ref. [25]. The atomic data for the reverse processes are obtained by detailed balance principle.

All atomic data can be readily obtained from the above theoretical framework [25] except for the photoexcitation cross section, which is derived from the oscillator strength f_{ij} for a dipole allowed transition from level i to j

$$\sigma_{ij}(h\nu) = \frac{\pi h e^2}{m_e c} f_{ij} S(h\nu), \tag{6}$$

where h is the Planck constant, m_e is the electron mass, $S(h\nu)$ is the line profile. A Voigt profile is utilized with natural lifetime broadening, Doppler and electron impact broadening being taken into account [15, 16].

Our recent work [26–29] showed that the direct double Auger decay, where two electrons are released simultaneously, played a role in the relaxation process and therefore we should include this process in the calculation. The direct double Auger decay rates are calculated by simplified formulas according to the knock-out (KO) and shake-off (SO) mechanisms

$$A^2_{KO} = \sum_m A^1_{im} \Omega_{mf}(\varepsilon_0) \tag{7}$$

and

$$A^2_{SO} = \sum_m A^1_{im} | < \Psi^{2+}_f | \Psi^+_m > |^2, \tag{8}$$

where A^1_{im} is the single Auger decay rate from the initial autoionizing level i to a middle level m, $\Omega_{mf}(\varepsilon_0)$ is the electron impact collision strength of the transition from the middle state m to the final state f at the incident energy ε_0. ε_0 is the Auger electron energy of the first single Auger decay process, which can be determined by the energy conservation law. The matrix element $| < \Psi^{2+}_f | \Psi^+_m > |$ is the overlap integral between the two wave functions determined in the field of the initial level and in the field of vacancies with two Auger electrons being emitted.

4. Results and discussions

We consider the population evolution of neon interacting with x-ray radiation at a photon energy of 1110 eV. We chose this photon energy for two reasons. On one hand, there are experimental results [6] to compare with. On the other hand, we are trying to develop a theoretical method to diagnose the radiation intensity or duration using the experiment as a reference. At 1110 eV, the photon can effectively ionize one $1s$ electron up to Ne^{6+}, while the $1s$ electron of higher ionization stages cannot be ionized by a single photon. Such a conclusion can be seen from our calculated ionization potentials (IPs) of $1s$ electron given in table 2. For comparison, the results from NIST [30], other theories [31] and experiments [32, 33] are also given wherever available.

A photon with energy of 1110 eV cannot ionize the $1s$ electron of Ne^{7+}, however, it can excite dipole allowed transitions of $1s \rightarrow 5p$ for Ne^{7+}. Although the resonances are weak and out of the central position of 1110 eV, they do play a role in the determination of CSD. Our calculated resonance position and oscillator strengths for some $1s \rightarrow 5p$ transitions are

given in table 3. Beyer *et al.* [31] reported the K x-ray transitions from highly charged neon ions (Ne^{7+}-Ne^{9+}) produced by heavy ion impact. To explain their experiment, they carried out theoretical calculations on the resonance energy of $1s \rightarrow np$ (n=2-7) by using multi-configuration Dirac-Fock method. Yet they use notation of LS coupling scheme to designate the lower and upper quantum states. Converting our jj coupling to the LS coupling, we can see that our calculated transition energies of $1s^2 2s \rightarrow 1s2s5p$ and $1s^2 2p \rightarrow 1s2p5p$ are in agreement with their results [31]. As the main focus of this work is to study the systematic trend of CSD with variation of the pulse intensity and duration, we do not give any detailed analysis on the resonance effects here.

The x-ray bandwidth depends on the electron bunch compression. In the experiments [3–11], the bandwidth is not accurately measured and the authors estimated it as ∼0.5%. Hence we take it to be 5.5 eV at the photon energy of 1110 eV. In the experiment, the high intensity is attained by tight focusing the x-ray beam to size ∼2 μm^2 [6]. To simplify the calculation, the x-ray spot is taken to be a circle with a diameter of 2 μm. As the rate coefficients due to photon processes are determined by the intensity, we solve the TDRE over a fine mesh of the space and time. The spatial step is taken to be $\delta r/\Delta$=0.1, which expands from the spot center r=0.0 to 3Δ. The time step is closely related with the intensity and it is fine to take the value of 1 fs at the peak intensity of 10^{18} W/cm^2. Figure 1 shows the fractional population evolution with time of different neon charge states irradiated by an x-ray beam with a duration of τ=75 fs and intensity of I_0=1.5×10^{17} W/cm^2 at the radial position r= (a) 0.0, (b) 1.0, and (c) 2.0 μm, respectively. It can easily be seen that the atomic neon is depleted after irradiation of 100 and 150 fs at r=0.0 and 1.0 μm, respectively. Yet the fraction of neon atom is about 20% at the end of the x-ray pulse at r=2.0 μm, which indicates the differences of CSDs at different positions of the laser spot. Therefore, one needs to integrate the population distributions in the spatial range of the laser spot in order to obtain a CSD that can be compared with the experiment. The fractional population as a function of time for different neon charge states averaged spatially over the x-ray laser spot are shown in Fig. 2.

In the experiment, Doumy *et al.* [6] measured the CSD using a Wiley-McLaren time-of-flight spectrometer. The pulse energy and electron bunch duration are measured to be 0.15 mJ and 100 fs, thus inferring the intensity of 2×10^{17} W/cm^2. As Young *et al.* [3] found from their experiment that the x-ray pulse duration is usually shorter than the electron bunch duration, resulting in an inaccuracy of the inferred intensity. Moreover, their CSD measurements are averaged over the space and time. In Fig. 3, we compared our theoretical CSD after further averaging over time for x-ray peak intensity of I_0=1.5×10^{17} W/cm^2 and duration τ=75 fs with the experimental and other theoretical results [6].

Doumy *et al.* [6] carried out two sets of theoretical calculations to explain their experiment by solving the rate equation. One is based on one-photon absorption cross sections and atomic relaxation rates obtained with Hartree-Fock-Slater approach [13]. The second one includes further shake-off processes as well as direct two-photon ionization of Ne^{8+}. The authors showed that the direct two-photon ionization played a trivial role if they utilized the cross section found in the literature. Therefore non-linear absorption is not a critical factor in the interaction processes. From the inspection of Fig. 3, our theoretical result and

their second set of calculation agree much better with their experiment. Such a conclusion is understandable as both theories include contributions from the direct double Auger processes. The effect of the direct double Auger processes can be found in detail in our recent work [29].

In the following, we point out that the CSD depends on the intensity and duration separately, not on the multiplication of them. As an example, we show in Fig. 4 the CSD at durations and intensities of 50 fs and 1.5×10^{17} W/cm^2, 75 fs and 1.0×10^{17} W/cm^2 and 150 fs and 5.0×10^{16} W/cm^2, respectively. The value of duration times intensity is the same for the three cases, while they show different population dynamics. For lower charge states from Ne^{1+} to Ne^{5+}, the results are basically the same for three cases. Yet differences are found for higher charge states. The longer the duration, the larger faction is found for Ne^{8+}. As a result, we should consider the CSD dependence on the intensity and duration separately.

The calculated CSD as a function of laser intensity from 1.0×10^{15} W/cm^2 to 1.0×10^{19} W/cm^2 is shown in Fig. 5 at the three durations: (a) 50, (b) 75 and (c) 100 fs, respectively. At the lowest intensity of 1.0×10^{15} W/cm^2, the CSD for the three durations differs very little. It is understandable as the x-ray radiation field at this intensity is basically a weak field and thus the interaction shows a typical physical picture of x-ray pulse photoionization of the neutral atomic neon. In this photoionization process, the $1s$ hole state $1s2s^22p^6$ of Ne^{1+} is effectively produced by x-ray photons and then it relaxes dominantly by Auger decay to Ne^{2+}. Another relaxation channel is the radiative decay, which is <2% of the total decay rate [34, 35], and thus resulting in a small fraction of Ne^{1+} and a large fraction (>70%) of Ne^{2+}. For the fraction of Ne^{3+}, the case is a little different. If only the photoionization process of the neutral atomic neon is considered, the population of Ne^{3+} is mainly produced by the direct double Auger decay [26–28]. Yet in the evolution with time, the effects of both direct double Auger decay and further ionization of Ne^{2+} are important in populating Ne^{3+}. Besides the K-shell photoionization of atomic neon, the photoionization of valence electrons of $2s$ and $2p$ plays a minor role as well. This latter process varies linearly with the intensity of the x-ray pulses, the population evolution does not vary much with the duration in the photoionization process. At the increased intensity of 1.0×10^{16} W/cm^2, this physical picture remains barely correct; however, new features appear. The fraction of Ne^{4+} begins to increase due to the x-ray radiation further ionizing $1s$ electron of Ne^{2+}. With the increase of intensity, however, the dominant processes occurring in the interaction change dramatically. From 1.0×10^{17} W/cm^2 up to higher intensity, the dominant ionization stages become the higher ionized ions of Ne^{7+} and Ne^{8+}, while the fractions of ions Ne^{3+}-Ne^{6+} are low for all laser duration and intensity studied here. The reason for this is that the dual process of photoionization followed by the Auger cascade becomes important. As we have discussed above, photons with an energy of 1110 eV can ionize the $1s$ electron from the neutral atom to Ne^{6+}. The lifetimes of these single core-hole states are small ($\sim$3 fs for Ne^{1+} to $\sim$10 fs for Ne^{6+} [3]) and thus upon photoionization the ion stages Ne^{3+}-Ne^{6+} decay to higher ionized ions via the Auger process. Hence the fraction of the Ne^{3+}-Ne^{6+} ions are always small. For Ne^{7+}, there is only a relatively weak resonance absorption channel and no effective direct photoionization channel can be accessed and thus a larger fraction than Ne^{3+}-Ne^{6+} can be found. As discussed in our previous work [12], after the resonance absorption of $1s \rightarrow 5p$

of Ne^{7+} the formed $1s$ excited state $1s2s5p$ will dominantly decay to the ground state of Ne^{8+}, which has no possible channel to Ne^{9+}. Therefore, the population distribution will mainly stay at the ground state of Ne^{8+}, which results in the large fraction of Ne^{8+}. Another trivial channel from Ne^{7+} to Ne^{8+} is the creation of excited states such as $1s2s$ and $1s5p$ by photoionization of valence electrons of $1s2s5p$. Such channels are too small to be observed at low intensity. However, it will become observable at higher laser intensity.

The CSD as a function of laser duration from 30 fs to 100 fs is shown in Fig. 6 at four intensity points of (a) 1.0×10^{16} W/cm^2, (b) 5.0×10^{16} W/cm^2, (c) 1.0×10^{17} W/cm^2, and (d) 1.0×10^{18} W/cm^2, respectively. At the intensity of 1.0×10^{16} W/cm^2, similar conclusions to those shown in Fig. 5 can be drawn. With the increase of intensity, the fraction of Ne^{2+} decreases, while the fraction of Ne^{7+} and Ne^{8+} increase, as discussed above. Moreover, with the increase of the x-ray pulse duration, this trend becomes more apparent, in particular for the fraction of Ne^{8+}.

5. Conclusion

The evolution of level population and CSD of neon interacting with x-ray pulses at a central photon energy of 1110 eV is investigated systematically by varying the intensity from 1.0×10^{15} W/cm^2 to 1.0×10^{19} W/cm^2 and duration from 30 fs to 100 fs with a Gaussian time profile and a circular spatial distribution for laser spot. At the intensity 1.5×10^{17} W/cm^2 and duration of 75 fs, the CSD evolution of different ionization stages with time is given as an example to show the dynamics at different distances from the spot center. By averaging over the spatial dimension of the laser spot, we determined the evolution dynamics with time for the fraction of all ionization stages from neutral atom to the bare ion. After further averaging over time, the CSD is compared with the experimental result and good agreement is found. By varying the laser intensity and duration, we systematically investigated the evolution of CSD. At intensity larger than 5.0×10^{16} W/cm^2, the evolution shows different features from the typical picture for a weak x-ray radiation field with the dominant ions being Ne^{2+} produced by the Auger decay of $1s$ hole state after absorption of the x-ray photon. The dominant ionization stages are Ne^{7+} and Ne^{8+}, while the fractions of Ne^{3+}-Ne^{6+} are comparatively small for all the laser pulse durations studied. Theoretical explanations are presented for such features.

Acknowledgment

This work was supported by the National Natural Science Foundation of China under Grants No. 11204376, No. 11274382 and No. 11274383. Calculations are carried out at the Research Center of Supercomputing Application, NUDT.

[1] P. Emma *et al.*, Nat. Photon. **4**, 641 (2010).
[2] T. Ishikawa *et al.*, Nat. Photon. **6**, 540 (2012).
[3] L. Young *et al.*, Nature (London) **466**, 56 (2010).
[4] M. Hoener *et al.*, Phys. Rev. Lett. **104**, 253002 (2010).
[5] L. Fang *et al.*, Phys. Rev. Lett. **105**, 083005 (2010).
[6] G. Doumy *et al.*, Phys. Rev. Lett. **106**, 083002 (2011).

[7] H. Thomas *et al.*, Phys. Rev. Lett. **108**, 133401 (2012).
[8] N. Rohringer *et al.*, Nature (London) **481**, 488 (2012).
[9] M. Nakano *et al.*, Phys. Rev. Lett. **110**, 163001 (2013).
[10] H. Fukuzawa *et al.*, Phys. Rev. Lett. **110**, 173005 (2013).
[11] S. Schreck *et al.*, Phys. Rev. Lett. **113**, 153002 (2014).
[12] W.J. Xiang, C. Gao, Y.S. Fu, J.L. Zeng, J.M. Yuan, Phys. Rev. A **86**, 061401(R) (2012).
[13] N. Rohringer, R. Santra, Phys. Rev. A **76**, 033416 (2007).
[14] O. Ciricosta, H.K. Chung, R.W. Lee, J. S. Wark, High Energy Density Phys. **7**, 111 (2011).
[15] J.L. Zeng, J.M. Yuan, Phys. Rev. E **74**, 025401(R) (2006).
[16] J.L. Zeng, J.M. Yuan, Phys. Rev. E **76**, 026401 (2007).
[17] J.L. Zeng, J. Phys. B: At. Mol. Opt. Phys. **41**, 125702 (2008).
[18] C. Gao, J.L. Zeng, Y.Q. Li, F.T. Jin, J.M. Yuan, High Energy Density Phys. **9**, 583 (2013).
[19] C. Gao, F.T. Jin, J.L. Zeng, J.M. Yuan, New J. Phys. **15**, 015022 (2013).
[20] S.J. Rose, High Energy Density Phys. **5**, 23 (2009).
[21] J. Bretagne, J. Godart, V. Puech, J. Phys. D: Appl. Phys. **15**, 2205 (1982).
[22] J. Abdallah Jr, J. Colgan, J. Phys. B: At. Mol. Opt. Phys. **45**, 035701 (2012).
[23] Y.P Liu, J.L. Zeng, J.M. Yuan, J. Phys. B: At. Mol. Opt. Phys. **46**, 145002 (2013).
[24] Y.P Liu, C. Gao, J.L. Zeng, J.M. Yuan, J.R. Shi, Astrophys. J. Supplement Series **211**, 30 (2014).
[25] M.F. Gu, Can. J. Phys. **86**, 675 (2008).
[26] J.L. Zeng, P.F. Liu, W.J. Xiang, J.M. Yuan, Phys. Rev. A **87**, 033419 (2013).
[27] J.L. Zeng, P.F. Liu, W.J. Xiang, J.M. Yuan, J. Phys. B: At. Mol. Opt. Phys. **46**, 215002 (2013).
[28] P.F. Liu, Y.P. Liu, J.L. Zeng, J.M. Yuan, Eur. Phys. J. D **68**, 214 (2014).
[29] C. Gao, J.L. Zeng, J.M. Yuan, Contrib. Plasma Phys. **55**, 123 (2015).
[30] Yu. Ralchenko, A.E. Kramida, J. Reader, and NIST ASD Team (2011). NIST Atomic Spectra Database (ver. 4.1.0), [Online]. Available: http://physics.nist.gov/asd [2012, May 1]. National Institute of Standards and Technology, Gaithersburg, MD.
[31] H.F. Beyer, K-H Schartner, F. Folkmann, J. Phys. B: Atom Molec. Phys. **13**, 2459 (1980).
[32] T.D. Thomas, R.W. Shaw, Jr., J. Electron Spectroscopy and Related Phenomena **5**, 1081 (1974).
[33] B. Bruch, D. Schneider, M.H. Chen, K.T. Chung, B.F. Davis, Phys. Rev. A **45**, 4476 (1992).
[34] C.P. Bhalla, J. Phys. B: Atom Molec. Phys. **8**, 1200 (1975).
[35] K.R. Karim, L. Logan, Physica Scripta. **58**, 574 (1998).

Table 1: The configurations of neon ions used in the present calculation. $(N)^M$ indicates the possible arrangement of the M electrons in the orbital with principle quantum number N.

Ion	Configuration
Ne	$(1)^2(2)^8$, $(1)^2(2)^7(3)^1$, $(1)^1(2)^8(3)^1$, $(1)^0(2)^8(3)^2$
Ne^{1+}	$(1)^2(2)^7$, $(1)^2(2)^6(3)^1$, $(1)^1(2)^8$, $(1)^1(2)^7(3)^1$, $(1)^0(2)^8(3)^1$
Ne^{2+}	$(1)^2(2)^6$, $(1)^2(2)^5(3)^1$, $(1)^1(2)^7$, $(1)^1(2)^6(3)^1$, $(1)^0(2)^8$, $(1)^0(2)^7(3)^1$
Ne^{3+}	$(1)^2(2)^5$, $(1)^2(2)^4(3)^1$, $(1)^1(2)^6$, $(1)^1(2)^5(3)^1$, $(1)^0(2)^7$, $(1)^0(2)^6(3)^1$
Ne^{4+}	$(1)^2(2)^4$, $(1)^2(2)^3(3)^1$, $(1)^1(2)^5$, $(1)^1(2)^4(3)^1$, $(1)^0(2)^6$, $(1)^0(2)^5(3)^1$
Ne^{5+}	$(1)^2(2)^3$, $(1)^2(2)^2(3)^1$, $(1)^1(2)^4$, $(1)^1(2)^3(3)^1$, $(1)^0(2)^5$, $(1)^0(2)^4(3)^1$
Ne^{6+}	$(1)^2(2)^2$, $(1)^2(2)^1(3)^1$, $(1)^2(2)^1(4)^1$, $(1)^1(2)^3$, $(1)^1(2)^2(3)^1$, $(1)^1(2)^2(4)^1$, $(1)^0(2)^4$, $(1)^0(2)^3(3)^1$, $(1)^0(2)^3(4)^1$
Ne^{7+}	$(1)^2(2)^1$, $(1)^2(3)^1$, $(1)^2(4)^1$, $(1)^2(5)^1$,$(1)^1(2)^2$, $(1)^1(2)^1(3)^1$, $(1)^1(2)^1(4)^1$, $(1)^1(2)^1(5)^1$, $(1)^0(2)^3$, $(1)^0(2)^2(3)^1$, $(1)^0(2)^2(4)^1$, $(1)^0(2)^2(5)^1$
Ne^{8+}	$(1)^2$, $(1)^1(2)^1$, $(1)^1(3)^1$, $(1)^1(4)^1$, $(1)^1(5)^1$, $(1)^0(2)^2$, $(1)^0(2)^1(3)^1$, $(1)^0(2)^1(4)^1$, $(1)^0(2)^1(5)^1$
Ne^{9+}	$(1)^1$, $(2)^1$, $(3)^1$, $(4)^1$, $(5)^1$

Table 2: The $1s$ ionization potential (IP) (eV) of the ground levels of Ne-Ne^{9+}.

Ion	Ground level	IP	Other work
Ne	$[(1s^22s^2)2p_{1/2}^2 2p_{3/2}^4]_0$	868.8	870.3[32]
Ne^{1+}	$[(1s^22s^2)2p_{1/2}^2 2p_{3/2}^3]_{3/2}$	892.6	
Ne^{2+}	$[(1s^22s^2)2p_{1/2}^2 2p_{3/2}^2]_2$	923.1	
Ne^{3+}	$[(1s^22s^2)2p_{1/2} 2p_{3/2}^2]_{3/2}$	957.9	
Ne^{4+}	$[(1s^22s^2)2p_{1/2}^2]_0$	1000.8	1001.8[33]
Ne^{5+}	$[(1s^22s^2)2p_{1/2}]_{1/2}$	1049.4	1048.5[33]
Ne^{6+}	$[(1s^2)2s^2]_0$	1099.5	1099.1[33]
Ne^{7+}	$[(1s^2)2s]_{1/2}$	1143.2	
Ne^{8+}	$[1s^2]_0$	1194.8	1194.7[31],1195.3[30]
Ne^{9+}	$[1s]_{1/2}$	1362.2	1362.3[31]

Table 3: Resonance position (RP) (eV) and weighted oscillator strengths (gf) of $1s \rightarrow 5p$ transitions from $1s^2 2s$ and $1s^2 2p$ configurations of Ne^{7+}, which are near the photon energy of 1110 eV. Only gf values larger than 0.001 are listed for convenience.

Lower level	Upper level	RP	gf
$[1s^2 2s_{1/2}]_{1/2}$	$[(1s_{1/2}2s_{1/2})_1 5p_{3/2}]_{3/2}$	1107.8	0.0394
$[1s^2 2s_{1/2}]_{1/2}$	$[(1s_{1/2}2s_{1/2})_1 5p_{3/2}]_{1/2}$	1107.8	0.0198
$[1s^2 2p_{1/2}]_{1/2}$	$[(1s_{1/2}2p_{3/2})_1 5p_{1/2}]_{3/2}$	1108.5	0.0095
$[1s^2 2p_{1/2}]_{1/2}$	$[(1s_{1/2}2p_{3/2})_1 5p_{1/2}]_{1/2}$	1108.5	0.0066
$[1s^2 2p_{1/2}]_{1/2}$	$[(1s_{1/2}2p_{3/2})_1 5p_{3/2}]_{3/2}$	1108.6	0.0038
$[1s^2 2p_{3/2}]_{3/2}$	$[(1s_{1/2}2p_{3/2})_1 5p_{1/2}]_{3/2}$	1108.3	0.0027
$[1s^2 2p_{3/2}]_{3/2}$	$[(1s_{1/2}2p_{3/2})_1 5p_{3/2}]_{5/2}$	1108.3	0.0201
$[1s^2 2p_{3/2}]_{3/2}$	$[(1s_{1/2}2p_{3/2})_1 5p_{1/2}]_{1/2}$	1108.3	0.0039
$[1s^2 2p_{3/2}]_{3/2}$	$[(1s_{1/2}2p_{3/2})_1 5p_{3/2}]_{3/2}$	1108.4	0.0182
$[1s^2 2p_{3/2}]_{3/2}$	$[(1s_{1/2}2p_{3/2})_1 5p_{3/2}]_{1/2}$	1108.9	0.0015

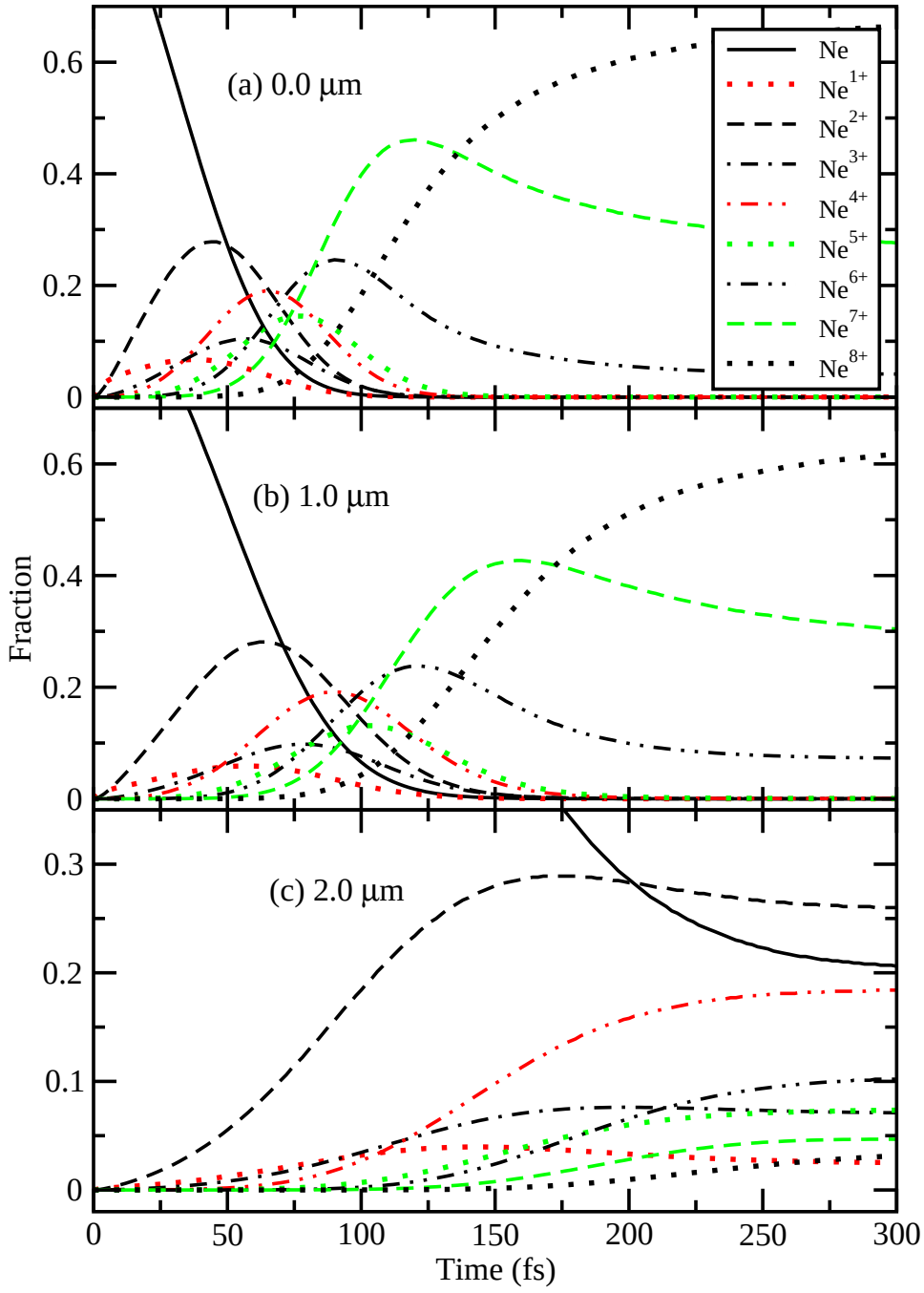

Figure 1: (Color online) Fractional population evolution of neon charge states interacting with an x-ray pulse at r= (a) 0.0, (b) 1.0 and (c) 2.0 μm. The parameters of the x-ray pulse is I_0=1.5×10^{17} W/cm^2, τ=75 fs and central photon energy $h\nu_0$=1110 eV, respectively.

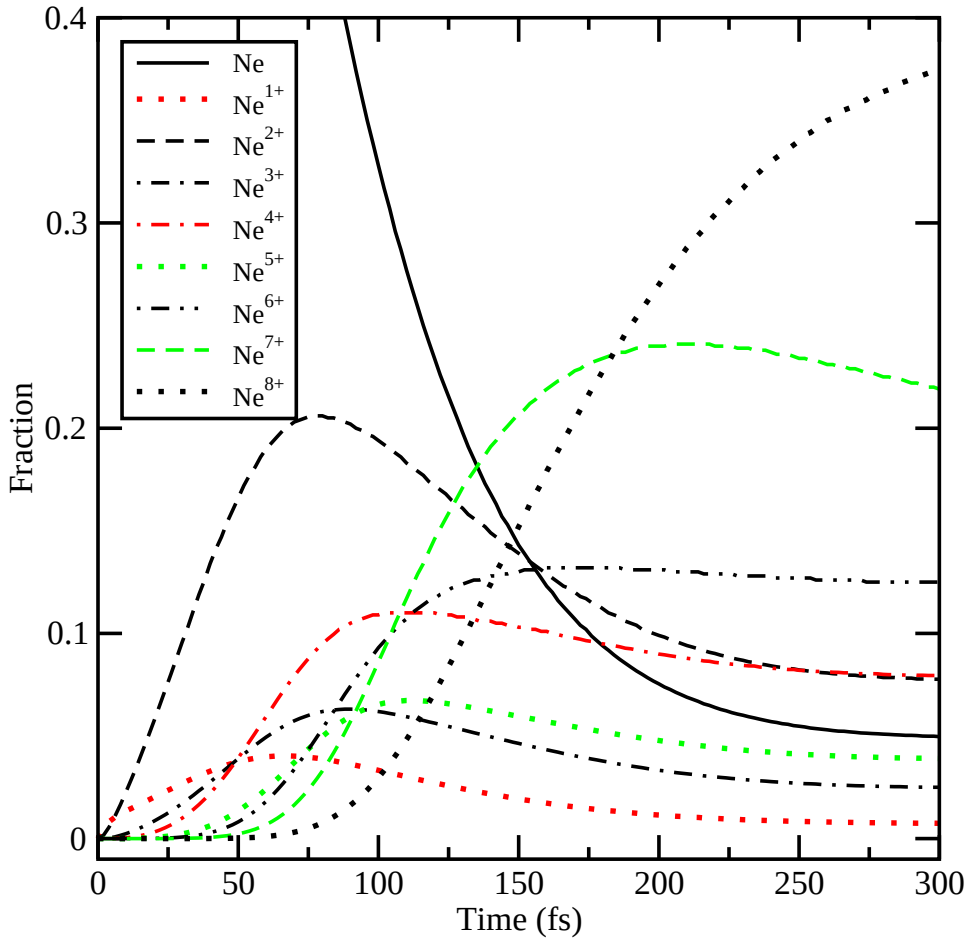

Figure 2: (Color online) Fractional population evolution of neon charge states interacting with an x-ray pulse after spatially averaging.

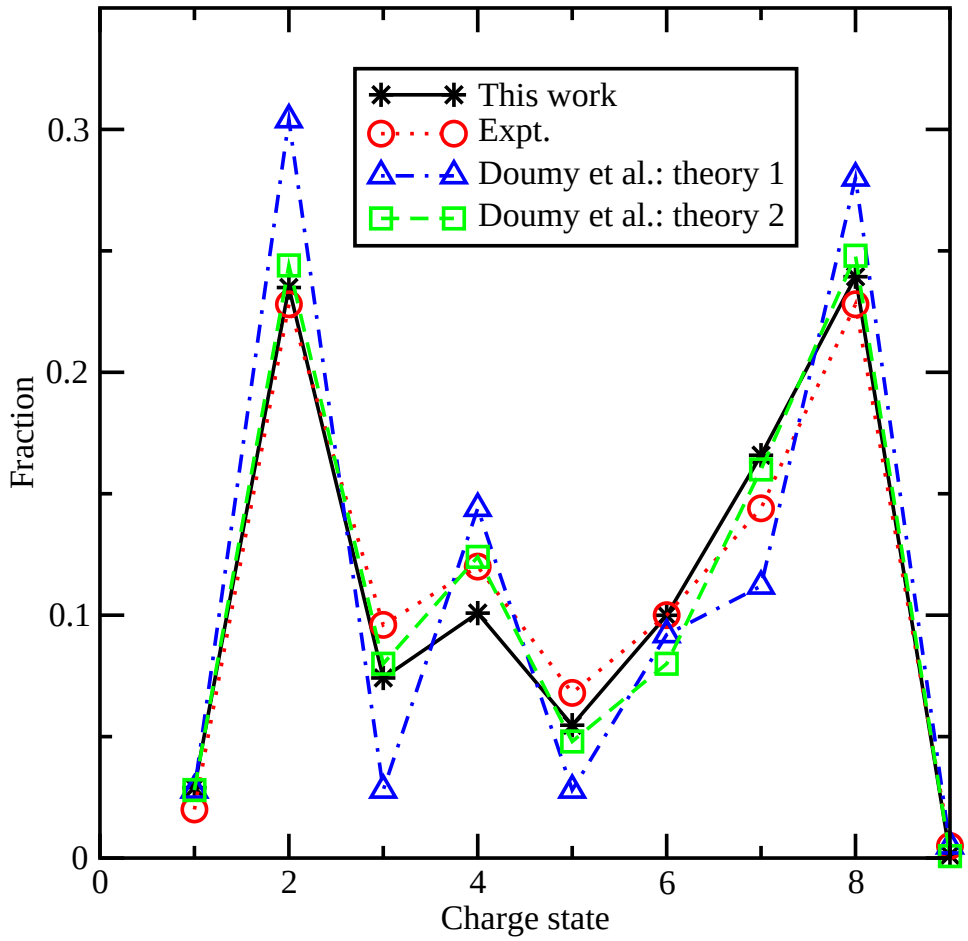

Figure 3: (Color online) CSD of neon interacting with x-ray pulses: comparison with the experimental data and previous theoretical results. The parameters of the x-ray pulse is I_0=1.5×10^{17} W/cm^2, τ=75 fs and $h\nu_0$=1110 eV to best fit the experimental result. The dot-dashed line with triangles represents the theoretical results reported in Ref. [6] by using the method developed by Rohringer in Ref. [13]. The dashed line with squares represents the result including further shake-off processes and direct two-photon ionization of Ne^{8+} [6].

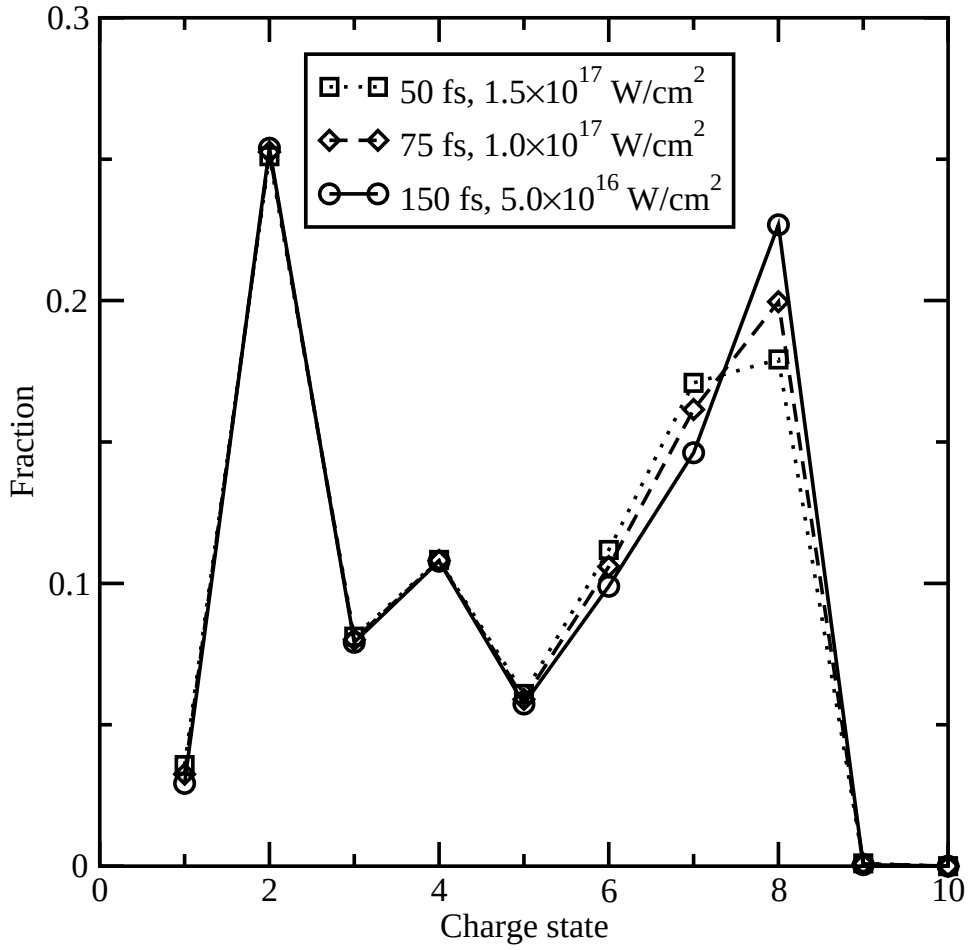

Figure 4: CSD of neon irradiated by x-ray pulses with the same value of $I_0 \times \tau$, i.e., 50 fs and 1.5×10^{17} W/cm^2 (dotted line with squares), 75 fs and 1.0×10^{17} W/cm^2 (dashed line with diamonds) and 150 fs and 5.0×10^{16} W/cm^2 (solid line with circles), respectively. The central photon energy of the x-ray pulse is $h\nu_0$=1110 eV.

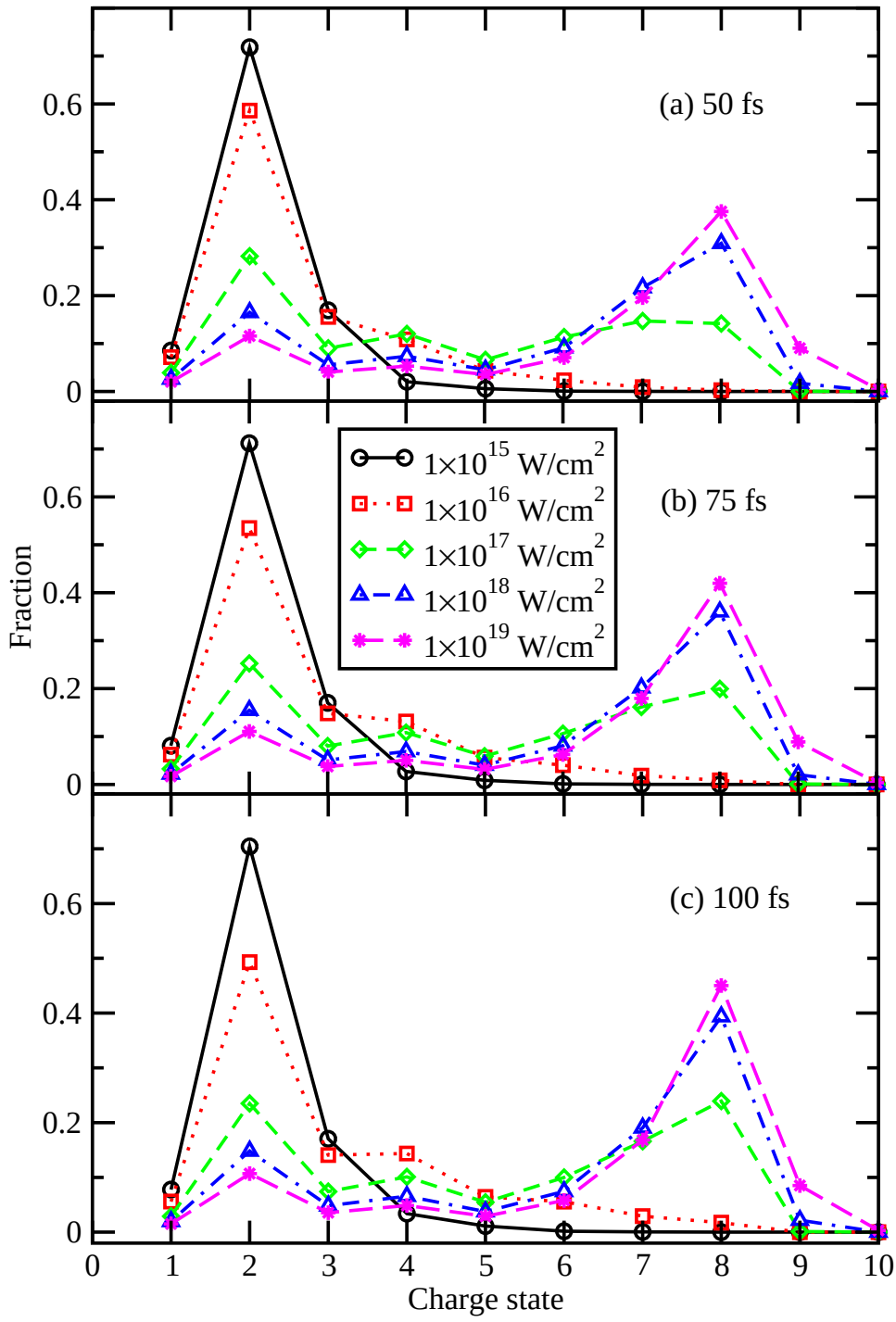

Figure 5: (Color online) CSD of neon interacting with x-ray pulses of $h\nu_0$=1110 eV and duration τ=(a) 50 fs, (b) 75 fs and (c) 100 fs, respectively. In each panel, the CSDs for a variety of peak intensity ranging from 1.0×10^{15} W/cm^2 through 1.0×10^{19} W/cm^2 are shown.

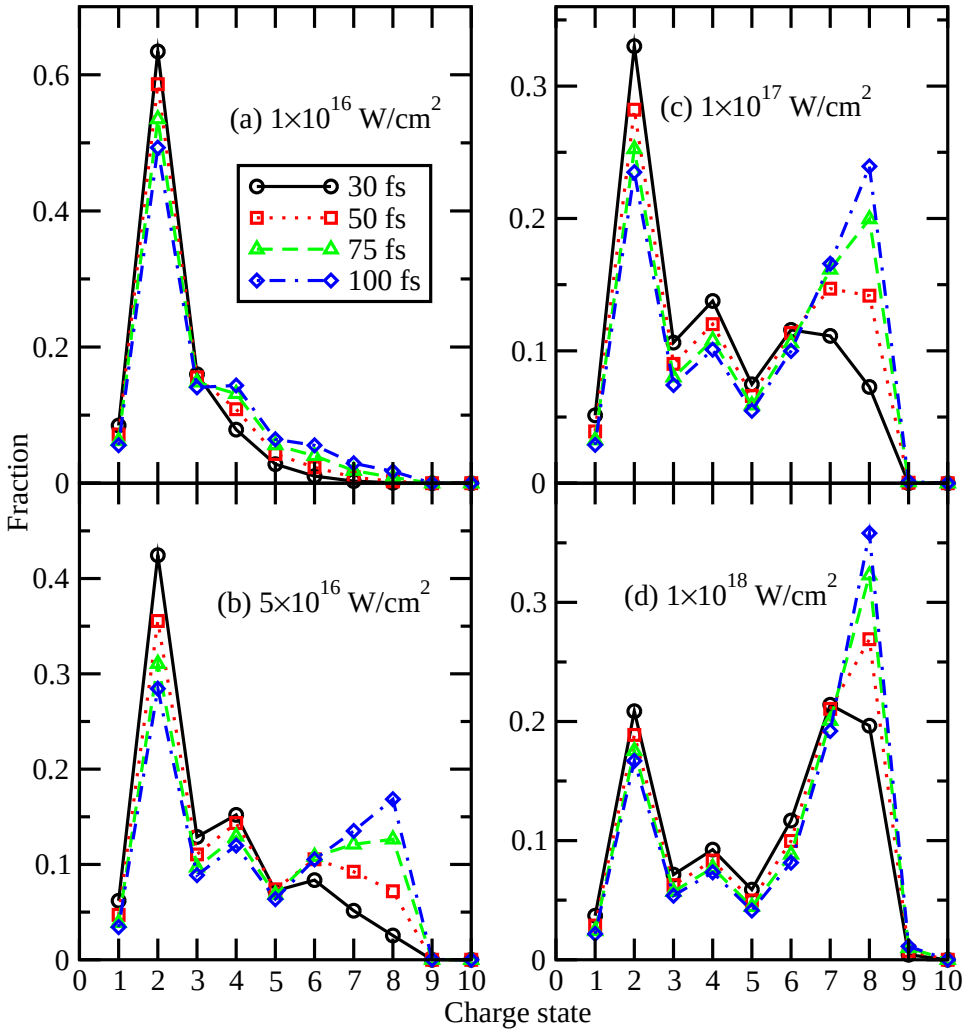

Figure 6: (Color online) CSD of neon interacting with x-ray pulses of $h\nu_0$=1110 eV and peak intensity I_0=(a) 1.0×10^{16} W/cm^2, (b) 5.0×10^{16} W/cm^2, (c) 1.0×10^{17} W/cm^2 and (d) 1.0×10^{18} W/cm^2, respectively. In each panel, the CSDs for a variety of duration τ ranging from 30 fs through 100 fs are shown.